Separation and Reconstruction of the Rigid Body and Micro-Doppler Signal in ISAR Part I – Theory

L. Stanković[1], S. Stanković[1], T. Thayaparan[2], M. Daković[1], I. Orović[1]

Abstract

In radar imaging, the micro-Doppler effect is caused by fast movements of some scattering points on the target. These movements correspond to highly non-stationary components in the time-frequency domain of the signal. The rigid body can be considered as stationary at one range location during the processing time. This property is used to separate the micro-Doppler signal from the rigid body using the L-statistics. Since the rigid body can be considered as a sparse signal, its values can be fully recovered at the positions where the micro-Doppler and rigid body components overlap. The recovery is based on the compressive sensing theory and methods.After an overview of the methods, a quantitative analysis of the improvements achieved in the time-frequency based separation is done. Also, a comparison with both the time and the frequency domain analysis is provided. Analysis of small additive noise influence to the reconstruction accuracy is done.

I. Introduction

In the inverse synthetic aperture radar (ISAR), the distance and the velocity component along the line-of-sight are used to locate the target point in the range/cross-range domain [1]–[4]. Since the range and cross-range information are contained within the frequencies of two-dimensional sinusoids, a common technique used in the ISAR signal analysis is the two-dimensional Fourier transform. Its application to the ISAR signal of a point target results in a highly concentrated function at a point whose position corresponds to the range and cross-range values [1], [3], [5], [6]. However, if there are some fast-moving parts on a target, they will produce fast frequency changes, causing micro-Doppler effects [1], [5], [7], [8]. These parts have increased speed, projecting themselves in a different scale in the ISAR image than the scale of slow-moving parts [9]. Micro-Doppler effect can also cover slow moving (rigid body) parts of a target and degrade the ISAR image. In addition, the micro-Doppler effect also contains useful information about the fast-moving parts of the target. The separation of patterns caused by rigid body parts of the target from the patterns caused by fast moving parts is an important topic in the ISAR (and SAR) signal analysis [4], [10]–[12]. The micro-Doppler effect in most cases is not well concentrated either in the time or in the frequency domain. However, this part of the signal is commonly well-concentrated in the time-frequency domain [13], [14]. Thus the separation of the micro-Doppler part and the rigid body part could be efficient in the time-frequency domain. A method for the

[1] Ljubiša Stanković, Srdjan Stanković, Miloš Daković, and Irena Orović are with University of Montenegro, Faculty of Electrical Engineering, 81000 Podgorica, Montenegro, E-mail: {ljubisa,srdjan,milos,irenao}@ac.me.

[2] Thayananthan Thayaparan is with Radar Applications and Space Technologies, Defence R&D Canada – Ottawa, Ottawa, Ontario, Canada, E-mail: Thayananthan.Thayaparan@drdc-rddc.gc.ca.

This research is supported by the Montenegro Ministry of Science project CS-ICT (Grant No. 01-1002).

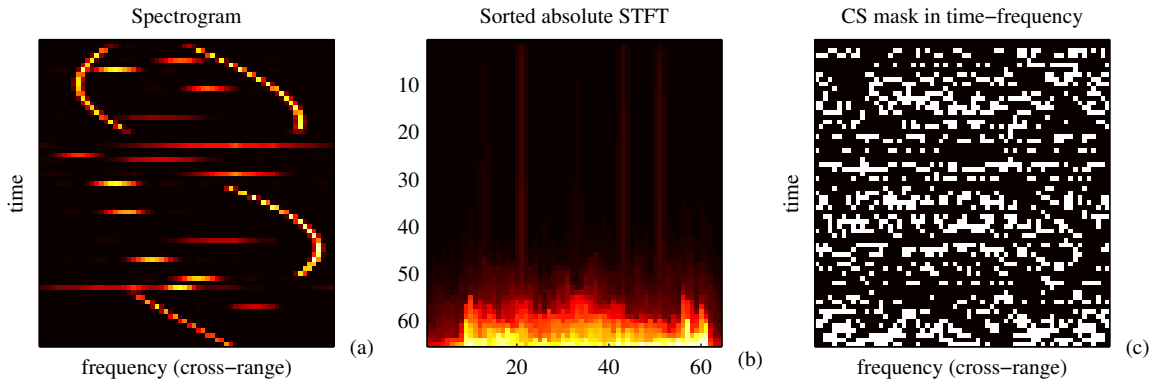

Fig. 1. Time-frequency representation of the radar signal, at a given range, corresponding to five rigid body points and four micro-Doppler reflectors, and several points reflecting during a short time interval, producing flashes: (a) The absolute STFT value within the coherent integration time, (b) The absolute STFT values, sorted along time, for each frequency (cross-range), (c) The matrix showing available (in white) and omitted (in black) values in the time-frequency plane, after the L-statistics approach with 60% of omitted values is used. The Hanning window is used in time-frequency analysis.

time-frequency domain based separation has been presented in [4]. The non-stationary parts of the radar signal are detected by using the L-statistics [15], [16] and they are removed from the time-frequency representation of the signal.

Of course some parts of the rigid body signal, overlapping in the time-frequency plane with the micro-Doppler effect, are also removed. Thus we are left with a reduced number of samples representing rigid body part of the signal, Fig.1. Since the rigid body signal can be considered as a sparse signal in the Fourier domain, the theory and reconstruction algorithms derived within compressive sensing (CS) theory [17], [18] can be used to recover the rigid body signal as if all signal samples where known and undisturbed [16], [19], [20]. After the rigid body signal is fully recovered, its separation from the micro-Doppler signal is straightforward.

In this paper, after a review of the separation and reconstruction methods, an analysis to the reconstruction process is done. The analysis is based upon the improvement that can be expected with respect to the case if all signal samples containing both the rigid body parts and micro-Doppler parts of the signal are removed in the time domain, before the reconstruction algorithm is applied. It is shown that the reconstruction based on the reduced set of samples in the joint time-frequency domain is significantly improved with respect to any of these domains considered separately.

The paper is organized as follows. In Section II, the time-frequency based separation of the rigid body and the Micro-Doppler effect are reviewed. The analysis of the recovery bounds by spark and restricted isometry property is done in Section III. A simple recovery algorithm is presented in Section IV.

II. Time-Frequency Based Separation

Let us consider a radar return signal after coherent processing and filtering, which consists of two sets of components

$$x(n) = x_{rb}(n) + x_{mD}(n). \tag{1}$$

One stationary set, whose frequencies may be considered as constant within the CIT, denoted by $x_{rb}(n)$. Components of this signal correspond to the rigid body

$$x_{rb}(n) = \sum_{i=1}^{K} \rho_i e^{j2\pi k_{0i} n/N} \tag{2}$$

at the cross-range positions (corresponding to the signal frequencies k_{0i}). The other set is nonstationary with components having fast frequency changes during the CIT. They are denoted by $x_{mD}(n)$. The assumption for this set of components is that their time-frequency representation (spectral content) is well concentrated in the joint-time frequency domain and that it changes over time.

As a time-frequency representation of these radar signals, containing the rigid body part and the micro-Doppler part, we will use the simplest and linear short-time Fourier transform (STFT) [21]. Its form with a rectangular window is

$$STFT(n,k) = \sum_{m=0}^{M-1} x(n+m)e^{-j2\pi mk/M}. \tag{3}$$

In a matrix form, it can be written as:

$$\mathbf{STFT}_M(n) = \mathbf{W}_M \mathbf{x}(n), \tag{4}$$

where $\mathbf{STFT}_M(n)$ and $\mathbf{x}(n)$ are vectors:

$$\begin{aligned} \mathbf{STFT}_M(n)&=[STFT(n,0),...,STFT(n,M-1)]^T, \\ \mathbf{x}(n)&=[x(n),x(n+1),...,x(n+M-1)]^T, \end{aligned} \tag{5}$$

and $\mathbf{W}_M$ is the $M \times M$ DFT matrix with coefficients $W(m,k) = \exp(-j2\pi km/M)$.

Frequency of the rigid body does not change so we may assume that the absolute value of

$$STFT_{rb}(n,k) = \sum_{m=0}^{M-1} x_{rb}(n+m)e^{-j2\pi mk/M}$$

is constant over time, for a given frequency,

$$|STFT_{rb}(n,k)| = C(k).$$

The micro-Doppler based part of the signal is spread over both time and frequency domain, considered separately, but well localized in the joint time-frequency domain. We will also assume that for each frequency there are at least some time instants during the CIT that are micro-Doppler free, i.e., $|STFT_{mD}(n,k)| = 0$. This kind of micro-Doppler effects can cover the whole rigid body in both time and frequency domains considered separately.

The result may easily be generalized for linear frequency changes of the rigid body components over the CIT by using the first order local polynomial Fourier transform (LPFT)

$$LPFT(n,k;\alpha) = \sum_{m=0}^{M-1} x(n+m)e^{j\alpha m^2}e^{-j2\pi mk/M}. \tag{6}$$

with appropriately adjusted modulation coefficient α [2], [4], [22].

For notation simplicity, assume first that the nonoverlapping STFT is used in the time-frequency analysis. The STFT values are calculated with step M in time n

$$\mathbf{STFT} = \left[\mathbf{STFT}_M(0)^T,\ \mathbf{STFT}_M(M)^T,\ ...\ ,\mathbf{STFT}_M(N-M)^T\right]^T$$

All STFT values are combined into one vector

$$\mathbf{STFT} = \mathbf{W}_{M,N}\ \mathbf{x}. \tag{7}$$

The $N \times N$ matrix $\mathbf{W}_{M,N}$ is formed as

$$\mathbf{W}_{M,N}= \begin{bmatrix} \mathbf{W}_M & \mathbf{0}_M & \cdots & \mathbf{0}_M \\ \mathbf{0}_M & \mathbf{W}_M & \cdots & \mathbf{0}_M \\ \vdots & \vdots & \ddots & \vdots \\ \mathbf{0}_M & \mathbf{0}_M & \cdots & \mathbf{W}_M \end{bmatrix}, \tag{8}$$

where $\mathbf{0}_M$ is a $M \times M$ matrix with all 0 elements. The signal vector

$$\mathbf{x} = [\mathbf{x}(0)^T,\ \mathbf{x}(M)^T, ..., \mathbf{x}(N-M)^T]^T = [x(0),\ x(1),\ ...,\ x(N-1)]^T$$

contains all signal values.

Note that we have used notation $STFT(n,k)$ for a scalar STFT value at a given time n and frequency k. The boldface notation $\mathbf{STFT}_M(n)$ with time argument is used to represent the STFT vector containing M frequencies at an instant n. Finally the boldface notation $\mathbf{STFT}$ without arguments is a vector of all STFT values for all frequencies k and all instants n.

We may write the signal vector $\mathbf{x}$ in terms of the DFT,

$$\mathbf{x} = \mathbf{W}_N^{-1}\mathbf{X}, \tag{9}$$

where $\mathbf{W}_N^{-1}$ denotes the inverse DFT matrix of the dimension $N \times N,$ while $\mathbf{X}$ is the DFT vector. Now, we have:

$$\mathbf{STFT} = \mathbf{W}_{M,N}\mathbf{W}_N^{-1}\mathbf{X} = \mathbf{\Psi X} \tag{10}$$

$$\mathbf{X}= \mathbf{W_N}\mathbf{W}_{M,N}^{-1}\mathbf{STFT}$$

In this case, the transformation matrix is defined as $\mathbf{\Psi}$ =$\mathbf{W}_{M,N}\mathbf{W}_N^{-1}$. It maps the global frequency information in $\mathbf{X}$ into the local frequency information in $\mathbf{STFT}$. The dimension of matrix $\mathbf{\Psi}$ is $N \times N$ and each of its rows corresponds to one STFT value $STFT(l) = STFT(n,k)$ with $l = n+k$ and $n \in \mathbb{N} = \{0, M, 2M, ..., N-M\}$ and $k \in \mathbb{K} = \{0, 1, 2, ..., M-1\}$. Obviously the inverse relation is $k = \mathrm{mod}(l, M)$ and $n = \mathrm{int}(l/M)$, where $\mathrm{mod}(l, M)$ and $\mathrm{int}(l/M)$ are the reminder and integer part, respectively, when l is divided by M.

The basic idea for separating the rigid body stationary signal and the micro-Doppler nonstationary signal is in the sorting of the STFT values along the time axis. Since the rigid body signal is stationary, the sorting procedure will not significantly change the distribution of its STFT values. However, the fast-varying micro-Doppler part of the signal is highly nonstationary, occupying different frequency positions for different time instants. Its existence is short in time, for each frequency, over a wide range of frequencies. Thus, after sorting the STFT along the time axis, the micro-Doppler nonstationary part of the signal have strong values at the wide frequency range, but for a few samples in sorted index only. By removing several strongest values of the sorted STFT, for each frequency, we eliminate most or all of the micro-Doppler nonstationary part of the signal. The rest of the STFT values contain the rigid body part of the signal only. Fast varying part of the signal, corresponding to micro-Doppler effect, can be detected and eliminated using the L-statistics [4], [19]. After the micro-Doppler part of the signal is removed, a part of the signal which overlaps with disturbance is removed as well. Therefore, just some of the desired sparse signal values are available for analysis and recovery process [19]. Here, a short review of the method from [19] will be presented.

By removing a set of time-frequency points using the L-statistics, only some elements in the observation vector $\mathbf{STFT}$ remain. Namely, for each frequency k, a vector of $\mathbf{STFT}$ in time is formed as:

$$\mathbf{S}_k = \{STFT(n,k),\ n = 0, M, 2M, ..., N-M\}. \tag{11}$$

After sorting the elements of $\mathbf{S}_k$, we obtain the new ordered set of STFT elements $\mathbf{S}_{k,sorted}$. A percentage Q of the high and low value elements are removed from consideration. These values capture most of the overlapping values of the rigid body and micro-Doppler effect in the time-frequency samples. The rest of the STFT values belong to the desired sparse rigid body signal.

Denote the vector of available STFT values by $\mathbf{STFT}_{CS}$. The values of elements of $\mathbf{STFT}_{CS}$ denoted by $STFT_{cs}(l)$ are

$$STFT_{cs}(l) = STFT(n_l, k_l)$$

for

$$(n_l, k_l) \in \mathbb{N}_A \subset \mathbb{N} \times \mathbb{K}$$

where $\mathbb{N} \times \mathbb{K}$ is the direct product (all pairs) of time instants used in calculation and frequencies from the STFT. The total number of the available elements (n_l, k_l) is $N_A = \text{card}\{\mathbb{N}_A\}$. Note that $\text{card}\{\mathbb{N} \times \mathbb{K}\} = N$ for N/M being an integer.

The same notation may be applied for the overlapping STFT. The only difference is that $\mathbf{STFT}_M(n) = \mathbf{W}_M\mathbf{x}(n)$ is calculated at $n \in \mathbb{N} = \{0, R, 2R, ..., N-R\}$ where $1 \leq R \leq M$ is the time step of the STFT calculation. In this case, the total number of calculated STFT values is $\text{card}\{\mathbb{N} \times \mathbb{K}\} = NM/R$.

The corresponding CS matrix $\mathbf{A}$, relating the sparse DFT vector $\mathbf{X}$ to $\mathbf{STFT}_{CS}$,

$$\mathbf{STFT}_{CS} = \mathbf{AX}$$

is formed by omitting the rows in

$$\mathbf{\Psi} = \mathbf{W}_{M,N}\mathbf{W}_N^{-1}$$

corresponding to the removed STFT values. When a value of $STFT(n_l, k_l)$ is removed as unavailable (disturbed) then the row $l = n_l + k_l$ is removed from the full matrix $\mathbf{\Psi}$, since each row corresponds to one time and frequency point (n, k).

The reduced observations, along with the sparse DFT domain, and their linear relationship provide a basis for the CS problem formulation and application of the CS methods in its solution. For the sparse rigid body signal, the solution is obtained from the problem defined as

$$\min \|\mathbf{X}\|_0 \quad \text{subject to } \mathbf{AX} = \mathbf{STFT}_{CS}. \tag{12}$$

where $\|\mathbf{X}\|_0$ is the number of nonzero values in $\mathbf{X}$. It is also called norm-zero of $\mathbf{X}$ although it does not satisfy the properties of a norm. When we solve this problem then the rigid body signal is

$$\hat{x}_{rb}(n) = \mathbf{W}_N^{-1}\mathbf{X}.$$

In minimization algorithms norm-zero is commonly replaced by norm-one and $\|\mathbf{X}\|_1$ is minimized instead of $\|\mathbf{X}\|_0$ in (12) [17], [18], [23],

$$\min \|\mathbf{X}\|_1 \text{ subject to } \mathbf{AX} = \mathbf{STFT}_{CS}.$$

The existence of solution of these minimization problems and their equivalence is studied next.

In the case of linear frequency modulated rigid part, the same procedure would be applied to the LPFT of signal $\mathbf{S}_k = \{LPFT(n, k; \alpha),\ n = 0, M, 2M, ..., N-M\}$.

III. Analysis within the CS Framework

A. Spark and Coherence

Since the DFT of the rigid body signal $\mathbf{X}$ is sparse with sparsity K then the sufficient condition for its reconstruction from the measurements $\mathbf{STFT}_{CS}$ taken using matrix $\mathbf{A}$ is that the spark of $\mathbf{A}$ and the sparsity K satisfy the condition.

$$K < \frac{1}{2}\text{spark}(\mathbf{A}).$$

The spark of matrix $\mathbf{A}$ is equal to the minimal number of columns which are not independent. The direct spark calculation is a very complex problem. The spark of matrix $\mathbf{A}$ can be related to the coherence index of the matrix $\mathbf{A}$, defined by

$$\mu(\mathbf{A}) = \max_{k \neq i} \left| \frac{\langle \mathbf{a}_k, \mathbf{a}_i \rangle}{\|\mathbf{a}_k\|_2 \|\mathbf{a}_i\|_2} \right| \tag{13}$$

where $\mathbf{a}_k$ and $\mathbf{a}_i$ are column vectors of the measurement matrix $\mathbf{A}$. The spark of $\mathbf{A}$ is then

$$\text{spark}(\mathbf{A}) \cong 1 + \frac{1}{\mu(\mathbf{A})}$$

with

$$K < \frac{1}{2}(1 + \frac{1}{\mu(\mathbf{A})}). \tag{14}$$

If the number of rigid body components within one range bin is, for example, $K = 3$ then the matrix $\mathbf{A}$ guaranties the reconstruction if $\mu(\mathbf{A}) > 1/6$. This is also computationaly complex, but feasible check of the solution since it requires inner product calculation of $N(N-1)/2$ pairs of columns of matrix $\mathbf{A}$. It is extremely conservative (sufficient) limit. It guaranties the recovery in the worst case for any combination of the available samples and rigid body positions. It will be used to comment the presented method.

Before we start the analysis for the presented matrix $\mathbf{A}$, recall first that for any matrix $\mathbf{A}$ with N columns and $N_A \leq N$ rows holds (Welch bound) [24]

$$\mu(\mathbf{A}) \geq \sqrt{\frac{N - N_A}{N_A\,(N-1)}}. \tag{15}$$

The equality holds for matrices that form an equiangular tight frame. For random positions of available rows, this bound can not be satisfied for all possible combinations of available rows of a deterministic matrix. The partial DFT matrix with a large number of columns for some specific combinations of rows can be treated as a rough approximation of an equiangular tight frame, since it will not significantly differ from the Paley equiangular tight frame [24]. For arbitrary combination of rows and the DFT matrix, the case with $N_A = N - 1$ (one eliminated sample) is the only satisfying the limit value. All other cases will produce a value of $\mu(\mathbf{A})$ above the Welch limit. The sparsity bound (maximal number of rigid body components) for some values of available samples N_A is given in Table I. For example, we can see that just one missing sample $N_A = N - 1$ will reduce the number of rigid body points that can be reconstructed from $K = N$ (if all samples are available) to $K < \frac{1}{2}(1 + N - 1) = N/2$, since the bound for $\mu(\mathbf{A})$ for $N_A = N - 1$ is $N - 1$. For $N = 1024$, it means that one missing sample reduces the number of nonzero values that can be reconstructed to $K < 512$, Table I (second column). For $N_A = N - 1$, the partial DFT matrix is an equiangular tight frame with $\mu(A) = 1/(N-1)$. Probability of this event is studied in detail in the part two [25]. For $N_A = N - 4$, in the same way we get $K < N/4$ since for large N we have $N_A\,(N-1) = (N-4)\,(N-1) \cong (N-1)^2$. As we see even a small the number of unavailable samples significantly reduces the number of nonzero values (rigid body points) that can be reconstructed, if the general theory bound is considered. This is not a problem in our application, since the number of rigid body components, in one range bin, is quite small, $K \ll N$.

TABLE I

SPARSITY BOUND CALCULATED USING COHERENCE INDEX WITH 100 RANDOM REALIZATIONS AND $N = 1024$

$\frac{N-N_A}{N}$	$\frac{1}{8}$	$\frac{1}{4}$	$\frac{1}{2}$	$\frac{3}{4}$
K CS theory bound	42	23	16	9
K DFT (STFT $M = 1$)	17	11	6	3
K STFT (OVLP $M = 32$)	18	12	7	4
K STFT (NOVLP DC $M = 32$)	25	15	9	5

A statistical check on the number of nonzero values K that can be reconstructed is preformed on the DFT matrix of the same order as the matrix that is going to be used in our STFT based analysis. It corresponds to the special case of one-sample window ($M = 1$) in the STFT analysis. The values of K bound obtained in 100 realizations with different available values and the DFT matrix is presented in Table I as well. The bound of K is calculated using a random set of N_A rows of the full matrix $\mathbf{W_N W}_{M,N}^{-1}$ to form matrix $\mathbf{A}$. Then for each pair of columns of matrix $\mathbf{A}$, denoted by $\mathbf{a}_k, \mathbf{a}_i$, the coherence index is calculated using (13). The bound for K is then the smallest integer satisfying (14).

The same analysis for K is done for the STFT based matrix. In addition to the already mentioned case $M = 1$, the case $M = 32$ is presented in Table I. The value of $\mu(\mathbf{A})$ is calculated for each combination of columns of $\mathbf{A}$ and a given random set of available values in each realization. Due to the STFT being used as the basic tool in the analysis, we concluded that by increasing the value of M the frequency resolution plays an important role, as in the case of the signal analysis using the STFT. In general, to reconstruct just a few nonzero values, for example with the STFT and $M = 32$, a large number of samples in needed. Two cases when the STFT based analysis can produce the resolution in the frequency domain close to the DFT are considered. In the first case we exclude the possibility of having close components. In the coherence analysis, it means to exclude the value of $\mu(\mathbf{A})$ for small $|i - j|$ corresponding to close components. The results obtained using this assumption are indicated by DC (distant components) in Table I. If a number of close rigid body points can be expected, so that the DFT resolution is required, the presented method can be used with the STFT with overlapping (OVLP) in time. It is even a more common way of the STFT calculation. All relations remain the same and the requirement that $|i - j|$ is small is not used. The results for maximal number of rigid body points K is presented in Table I for all of these cases and $N_A = 7N/8$, $N_A = 3N/4$, $N_A = N/2$, and $N_A = N/4$. The case of $N_A = N/2$ means that in a half of the STFT values the rigid body and the micro-Doppler effect are overlapped in time-frequency domain. This is quite pessimistic assumption, along with very pessimistic estimation of the value of K based on the spark analysis. Thus in reality we can expect much better performance, although these are already sufficient for ISAR data analysis where the number of rigid body components, in one range bin, is quite small, $K \ll N$.

B. Restricted Isometry Property

Note that the other commonly used method to establish the solution existence is based on the restricted isometry property of matrix $\mathbf{A}$. The restricted isometry in this case would guaranty a solution if there is a restricted isometry constant δ_K such that

$$\left| \|\mathbf{AX}\|_2^2 - \|\mathbf{X}\|_2^2 \right| < \|\mathbf{X}\|_2^2 \, \delta_K$$

for $0 \leq \delta_K < 1$. This should be checked for all possible positions of K nonzero values (possible rigid body positions) in $\mathbf{X}$. The solution is unique if for a $2K$ sparse rigid body signal the restricted isometry property holds. Check of this condition is an NP hard problem that can not be implemented on computers for any reasonable values of N and K. For example, for

$N = 1024$ and $K = 4$ rigid body points, it would require the restricted isometry check for all possible combinations of $2K = 8$ columns out of the total number of $N = 1024$ columns of matrix $\mathbf{A}$. The number of combinations is $\binom{1024}{8} \sim 10^{20}$. For each of them, an eigenvalue analysis of a matrix should be done.

Here we will reformulate the restricted isometry property to the form that can easily be checked in the solution of the presented separation problem. We will assume that the measurement matrix is normalized in order to obtain isometry $||\mathbf{\Psi X}||_2 = ||\mathbf{X}||_2$ for full transformation matrix. In our case, this results in normalizing STFT values with factor $\sqrt{N/M}$. Now we have

$$\|\mathbf{AX}\|_2^2 = \|\mathbf{STFT}_{CS}\|_2^2 = \sum_{(n,k)\in\mathbb{N}_A}\sum |STFT(n,k)|^2 = \sum_{(n,k)\in\mathbb{N}_A}\sum SPEC(n,k)$$

where $SPEC(n,k)$ is the spectrogram and the summation goes over the available samples. Also Parseval's theorem holds for the normalized nonoverlapping STFT

$$\|\mathbf{STFT}\|_2^2 = \sum_{k=0}^{M-1}\sum_{n\in\mathbb{N}} |STFT(n,k)|^2 =$$

$$= \frac{N}{M}\sum_{k=0}^{M-1}\sum_{n\in\mathbb{N}}\sum_{m_1=0}^{M-1}\sum_{m_2=0}^{M-1} x_{rb}(n+m_1)x_{rb}(n+m_2)e^{-j2\pi(m_1-m_2)k/M}$$

$$= N\sum_{m=0}^{M-1}\sum_{n\in\mathbb{N}}|x_{rb}(n+m)|^2 = N\sum_{n=0}^{N-1}|x_{rb}(n)|^2 = \|\mathbf{X}\|_2^2 .$$

Therefore

$$\left|\frac{\|\mathbf{AX}\|_2^2 - \|\mathbf{X}\|_2^2}{\|\mathbf{X}\|_2^2}\right| = \frac{\sum\sum_{(n,k)\in(\mathbb{N}\times\mathbb{K})\setminus\mathbb{N}_A} SPEC(n,k)}{\|\mathbf{STFT}\|_2^2}.$$

It means that the restricted isometry property is satisfied with small δ_K if the ratio of the sum of spectrograms over the removed points and the sum over all points (energy of signal multiplied by N) is small. For the largest possible value of sparsity K when the restricted isometry can be checked, $2K = N$, it means that this ratio should be calculated over all possible values of $k \in \mathbb{N}$. It obviously means that if we remove all STFT values containing our signal $x_{rb}(n+m_1)$ energy, then the reconstruction is not possible independently of the number of remaining STFT values. Since in the L-statistics based approach the same number of STFT values is removed at all frequencies, then this situation is not possible, assuming that the rigid body is stationary over time and that the energy over all time points is uniformly distributed. Then the common restricted isometry condition $\delta_{2K} < \sqrt{2}-1$ (providing equivalence of norm-one and norm-zero solutions) will require that the energy of the removed STFT values is lower than $(\sqrt{2}-1)\|\mathbf{STFT}\|_2^2$, meaning $(N - N_A) < (\sqrt{2}-1)N$ or $N_A > (2-\sqrt{2})N = 0.59N$. The result that the signal of sparsity $K < N/2$ can be reconstructed if $N_A > 0.59N$ seems very optimistic with respect to the spark and coherence analysis. However, it has been derived with the assumption that the spectrogram (square modulus of the STFT) of a rigid body is constant over time. It means that there is no cross-terms in the spectrogram, requiring that the components are not to close to each other. However, if this assumption is not used the spectrogram of two close components is not constant over time and we will come to the number of rigid body points that can be reconstructed similar to the bound values obtained by using the coherence and spark analysis.

Example 1: Applying the presented procedure the rigid body part of the signal presented in the Fig. 1 (as illustrative example) is reconstructed. The rigid body consists of five scattering points with amplitudes $\rho_1 = 0.35$, $\rho_2 = 1.2$, $\rho_3 = 0.33$, $\rho_4 = 0.9$, and $\rho_5 = 1$. The Fourier transform of the input signal, the rigid body signal after the L-estimation (corresponding to norm-two minimization), and the signal after the presented reconstruction are shown in Fig. 2. The amplitudes and phase of the reconstructed signal are the same as the corresponding rigid body parameters. Since the reconstruction is complete, including

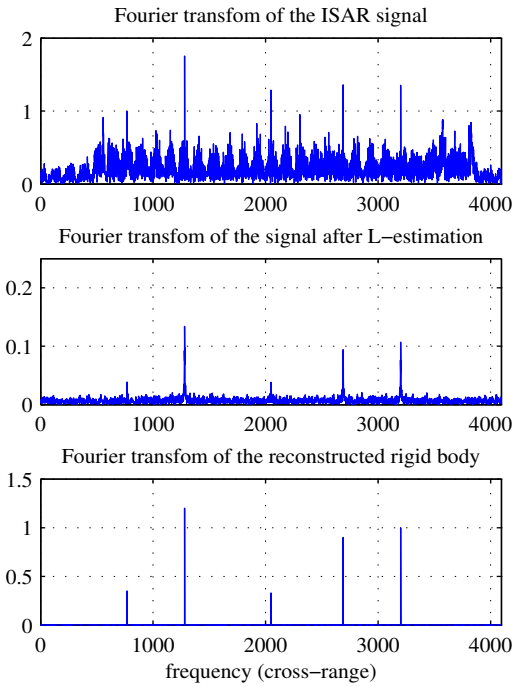

Fig. 2. The discrete Fourier transform (DFT) of the input signal (top), the rigid body signal after the L-estimation (middle), and the signal after the presented reconstruction (bottom). The DFT values are scaled with N to produce the signal component amplitudes ρ_i.

the phase of the components, the micro-Doppler part of the signal can be obtained by simple subtraction. The Hanning window is used in time-frequency analysis with STFT overlapping for $M/2$. Analysis may reduce to the two sets of nonoverlapping data as presented in [4], [19], [21].

Example 2: In this example, the real radar data corresponding to two outside corner reflectors, rotating at approximately $40\,\mathrm{rpm}$ (all facing radar) with rigid body, are analyzed within one range bin. In addition to one existing rigid body four rigid body components are added to be able to check the result. The STFT representation of the observed signal is shown in Fig. 3(a). The sorted STFT is shown in Fig. 3(b). The original DFT is shown in Fig. 3(c). The reconstructed Fourier transform of the rigid body, obtained by summing 40% of the remaining STFT values, after sorting in time, is presented in Fig. 3(d).

IV. Recovery Algorithm for the Rigid Body Signals

The goal is to reconstruct the original sparse stationary signal, producing the best concentrated DFT $X(k)$, using the available STFT values. Therefore, the corresponding minimization problem can be defined as follows:

$$\min \|\mathbf{X}\|_1 = \min \sum_{k=0}^{N-1} |X(k)| \qquad (16)$$

$$\text{subject to } \mathbf{STFT}_{CS} = \mathbf{A}\,\mathbf{X}.$$

Based on the values of $\mathbf{STFT}_{CS}$, the missing STFT values can be reconstructed such as to provide minimal $\sum_{k=0}^{N-1} |X(k)|$.

Here we will present a simple reconstruction algorithm with the L-estimation (norm-two solution) as the initial representation. This algorithm is a variant of the matching pursuit algorithms. The initial estimate of the Fourier transform of the rigid body is the solution of the norm-two minimization problem

$$\min \|\mathbf{X}\|_2 \text{ subject to } \mathbf{A}\,\mathbf{X} = \mathbf{STFT}_{CS}.$$

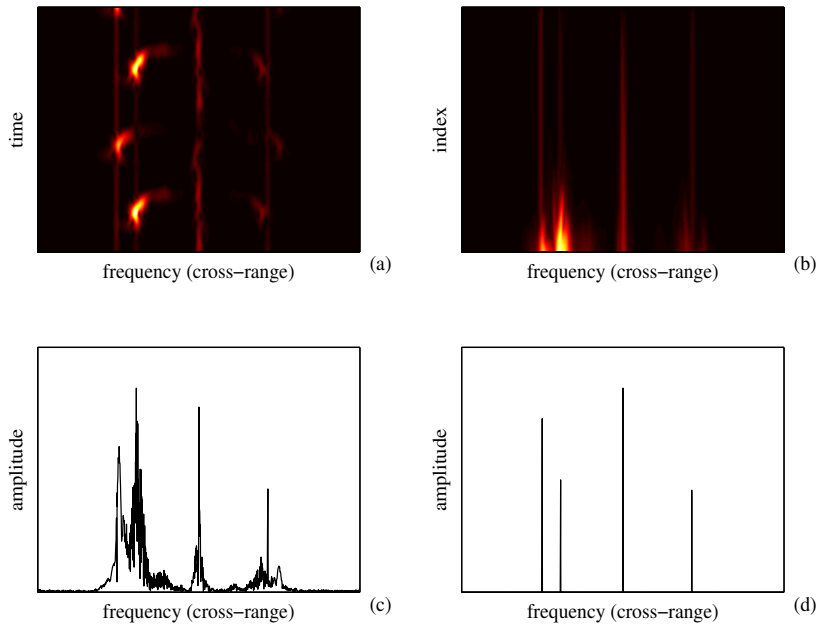

Fig. 3. Radar data corresponding to a rigid body and three corner reflectors rotating at ~ 60 RPM. (a,) The STFT. (b) The sorted STFT. (c) The original Fourier transform. (d) The Fourier transform reconstructed by summing over 40% of the lowest STFT samples and applying the reconstruction algorithm.

It corresponds to using zero values for unavailable STFT values. Two possibilities may occur. One is that all K positions of nonzero values of $\mathbf{X}$ can be detected based on the initial estimation. Then we will have a system with N_A linear equations and $K \ll N_A$ unknowns in $X(k)$, at the estimated positions, since all other values of $X(k)$ are assumed to be zero-valued. This vector is denoted by $\mathbf{X}_K$. Its values are $X_K(k) = 0$ for $k \notin \mathbb{K} = \{k_{01}, k_{02}, ...k_{0K}\}$. Now the system with K unknowns is

$$\mathbf{A}_K \mathbf{X}_K = \mathbf{STFT}_{CS}. \tag{17}$$

Matrix $\mathbf{A}_K$ is obtained from the matrix $\mathbf{A}$ by removing all columns at the positions of zero values in $X(k)$. This method can be used with both overlapped and nonoverlaped STFT values.

The algorithm can be summarized as follows:

(i) Calculate the initial transform estimate $X_2(k)$ by using the available/remaining STFT values and assuming that unavailable signal values are zero. This vector will be denoted by $\mathbf{STFT}^0_{CS}$.

$$\mathbf{X}_2 = \mathbf{W_N} \mathbf{W}^{-1}_{M,N} \mathbf{STFT}^0_{CS}. \tag{18}$$

This kind of calculation can be simplified, since the DFT can easily be reconstructed directly from the STFT. It is assumed that the STFT is calculated with such a window and time step that classical STFT to signal reconstruction condition is satisfied [21].

(ii) Find all positions k_{0i}, $i = 1, 2, \ldots, K_0$ where $|X_2(k_{0i})| > T_r$ is satisfied. Set the transform values $X(k)$ to zero at all positions k where initial estimate $X_2(k)$ is below a threshold T_r,

$$X(k) = \begin{cases} 0 & \text{for } k \neq k_{0i},\ i = 1, 2, ..., K_0 \\ X_2(k) & \text{for } k = k_{0i},\ i = 1, 2, ..., K_0 \end{cases} \tag{19}$$

This criterion is not sensitive to T_r as far as all nonzero positions of the original transform are detected and the total number K_0 of transform values in $X(k)$ satisfies the condition for a unique solution.

(iii) After their positions are detected in (ii), the unknown values of nonzero coefficients could be easily calculated by solving the set of N_A equations for available instants $n \in \mathbb{N}_A$, at the detected nonzero candidate positions k_{0i}, $i = 1, 2, ..., K_0$, using system (17). This system is solved in the least square sense as

$$\mathbf{X}_K = \left(\mathbf{A}_K^* \mathbf{A}_K\right)^{-1} \mathbf{A}_K^* \mathbf{STFT}_{CS}. \tag{20}$$

The reconstructed coefficients $X(k_{0i})$, $i = 1, 2, ..., K_0$, (denoted by vector $\mathbf{X}_K$) are exact and unique if the reconstruction conditions, discussed in the previous Section, are meet. If among the K_0 nonzero candidates in (20), there are some coefficients that should be zero valued, the system solution will provide correct (zero) values.

(iv) The reconstruction can be verified by recalculating back the STFT values using the reconstructed DFT vector $\mathbf{X}_R$ with components

$$X_R(k) = \begin{cases} 0 & \text{for } k \neq k_{0i},\ i = 1, 2, ..., K_0 \\ X_K(i) & \text{for } k = k_{0i},\ i = 1, 2, ..., K_0 \end{cases}$$

as $\mathbf{STFT}_R = \mathbf{W}_{M,N} \mathbf{W}_N^{-1} \mathbf{X}_R$. If the reconstruction error at the available positions

$$e = \|\mathbf{STFT}_R - \mathbf{STFT}_{CS}\|_2$$

calculated for the points $(n_l, k_l) \in \mathbb{N}_A$ is not zero (or bellow expected precision) then it means that we have not detected all rigid body candidates. We should form a residual STFT as $\mathbf{STFT}_{CS}^1 = \mathbf{STFT}_{CS}^0 - \mathbf{STFT}_R$ at the available points $(n_l, k_l) \in \mathbb{N}_A$ and go back to (i). Detect new possible candidates $k_{0(K+i)}$ and try to solve the problem (20) with new set of possible positions which is a set union of the positions detected in the initial step and using $\mathbf{STFT}_{CS}^1$. This procedure should be continued until the desired precision is satisfied or the allowed number of iterations is reached.

A special case of this procedure is one-by-one matching pursuit method when only the position of the largest value of the estimated DFT is used in each iteration. Then the detection step (19), in each iteration, is redefined as

$$X(k) = \begin{cases} 0 & \text{for } k \neq k_0 \\ X_2(k) & \text{for } k = k_0 \end{cases} \tag{21}$$

$$k_0 = \arg\{\max |X_2(k)|\}.$$

In this case there is no need for threshold.

Again in each next iteration, the union of the detected positions in the all previous and the current iteration is used. These two approaches produce similar results.

If the number of available samples is sufficiently large (much larger than the signal sparsity) then the solution producing zero (bellow desired precision) error will be unique with a high probability. Strict bounds for the uniqueness of the solution are defined by the spark or restricted isometry property. Their check is, in general an NP hard (computationally not feasible) problem. In addition, they offer very pessimistic bounds, including some zero probability events that are discussed in part II of this manuscript [25].

A. Additive Noise Influence

In the case of noisy STFT values the reconstruction is based on $\mathbf{STFT}_{CS} + \mathbf{STFT}_{CSN}$ where $\mathbf{STFT}_{CSN}$ is the STFT of additive noise [26]. Note that is corresponds to the STFT of input noise since the STFT is a linear transformation. If the variance of input white noise is σ_ε^2 then the variance of its STFT values is $E_w \sigma_\varepsilon^2$ where $E_w = M$ is the energy of rectangular window. For nonoverlapping windows noise in the STFT is uncorrelated, while for the case of overlapping windows the correlation

is a function of the overlapping interval. Since the algorithm reconstruction bounds will be considered in the second part of this paper, assume here that the amount of noise is such that it influences the algorithm accuracy only. At a signal component frequency $k = k_{0i}$ all available STFT values will sum up to produce $X(k_{0i})$. Consider the case when L-statistics is used and a constant number of STFT elements $M_A = MN_A/N$ is used in reconstruction for each instant. Then the initial DFT calculation $\mathbf{X}_2 = \mathbf{W_N}\mathbf{W}_{M,N}^{-1}\mathbf{STFT}_{CS}^{0}$ will produce the signal component at $k = k_{0i}$ whose amplitude is $\rho_i N M_A/M$, where ρ_i is the component amplitude. The variance of STFT noise $M\sigma_\varepsilon^2$ in the initial DFT calculation is added up $\frac{N}{M}\frac{M_A}{M}$ times instead of N/M is all STFT were available. When the frequencies are correctly detected based on the initial DFT calculation, then during the reconstruction process $\mathbf{X}_K = \left(\mathbf{A}_K^*\mathbf{A}_K\right)^{-1}\mathbf{A}_K^*\mathbf{STFT}_{CS}$ the amplitudes ate scaled to their correct values $N\rho_i$. The scaling factor is M/M_A. This scaling will be applied to the noise at $k = k_{0i}$ as well since

$$\left(\mathbf{A}_K^*\mathbf{A}_K\right)^{-1}\mathbf{A}_K^*(\mathbf{STFT_{CS}} + \mathbf{STFT_{CSN}}) = \mathbf{X}_K + \mathbf{X}_{\varepsilon K}$$

where $\mathbf{X}_{\varepsilon K}$ is the noise in reconstructed DFT. The reconstructed noise at the frequency $k = k_{0i}$ will be scaled in amplitude in the same way as the signal amplitude, by factor M/M_A. It means that the variance of noise in nonoverlapping case will be scaled with respect to the original variance $M\sigma_\varepsilon^2$ as

$$\mathrm{var}\{X(k_{0i})\} = \left(\frac{M}{M_A}\right)^2 M\sigma_\varepsilon^2\frac{N}{M}\frac{M_A}{M}. \tag{22}$$

The variance will decrease as the number of available samples M_A increases. Since only K_0 values of $X(k)$ different from zero will be used in the signal reconstruction it means that the reconstructed signal in time domain $x_R(n)$ will contain noise of variance

$$\mathrm{var}\{x_R(n)\} = \frac{1}{N^2}\sum_{i=1}^{K_0}\mathrm{var}\{X(k_{0i})_{\varepsilon K}\} = \frac{M}{M_A}\frac{K_0}{N}\sigma_\varepsilon^2. \tag{23}$$

With respect to the estimated number of components K_0 we should keep its value as small as possible in order to reduce the total noise in the reconstructed signal. Note that for $K_0 = N$, $M_A = M$ and rectangular nonoverlapping window the original variance of noise σ_ε^2 is obtained for $x_R(n)$.

Obtained relation is statistically checked on a signal with $N = 256$ and $K = 3$ signal components, using the STFT with $M = 16$ and assuming that 50% of data are removed at each time instant. The calculation is run on a signal $x(n) = 1.25\exp(2\pi k_{01}nN + \varphi_1) + \exp(2\pi k_{02}nN + \varphi_2) + 0.75\exp(2\pi k_{03}nN + \varphi_3) + \varepsilon(n)$, with 100 independent realization with various missing data sets and frequency positions. Standard deviation of the input noise is $\sigma_\varepsilon = 1$. Input signal-to-noise ratio is 5 [dB]. Statistically obtained variance of the reconstructed signal is $\mathrm{var}\{x_R(n)\} = 0.0238$, while expression (23) produces $\mathrm{var}\{x_R(n)\} = 0.0234$ corresponding to the output signal-to-noise ratio of 11.25 [dB]. Although the total signal-to-noise ratio is reduced in the reconstructed signal (mainly to the sparsity assuming that $N - K$ DFT values are zero), the variance of noise in a single DFT value $X(k_{0i}$, defined by (22) as $\mathrm{var}\{X(k_{0i})_{\varepsilon K}\} = \sigma_\varepsilon^2 NM/M_A$ is increased for the factor of M/M_A with respect to the case when all data are available, as expected. Illustration of the statistical analysis on one signal realization is presented in Fig.4.

V. Conclusion

ISAR signals containing the rigid body and micro-Doppler effect caused parts are considered. It has been assumed that these two parts of signal partially overlap in the time-frequency plane. After the detection and removal of overlapping values, a possibility and method for the full recovery of the rigid body signal are discussed. The property that the rigid body part of the signal can be considered as a sparse signal is used. The recovery of the rigid body is based on the compressive sensing

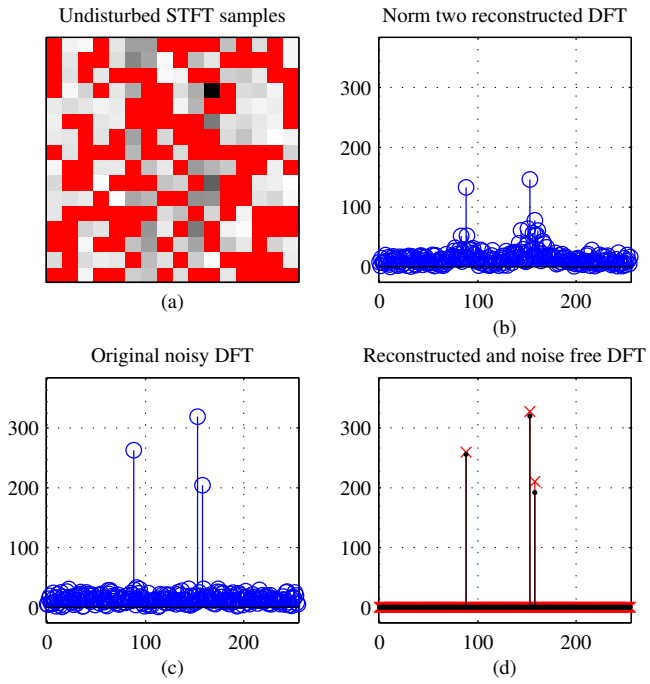

Fig. 4. Illustration of the statistical noise analysis on one signal realization: (a) Undisturbed rigid body STFT samples (disturbed and omitted values are in red). (b) The DFT of reconstructed rigid body using norm-two. (c) The DFT of original noisy rigid body signal. (d) Reconstructed DFT (denoted by x) and true noise free values (denoted by dot).

methods. The analysis of the performance of these methods is done, along with a simple recovery algorithm. The influence of a small additive noise to the reconstruction is analyzed.

REFERENCES

[1] Chen, V.C., Tahmoush, D., and Miceli, W.J.: 'Radar Micro-Doppler Signatures: Processing and Applications' (IET, 2014)

[2] Peng, S.B., Xu, J., Peng, Y.N., Xiang, J.B.: 'Parametric inverse synthetic aperture radar maneuvering target motion compensation based on particle swarm optimizer', IET Radar Sonar and Navigation, 2011, **5**, (3), pp 305–314

[3] Stove, A.G.: 'Linear FMCW radar techniques', IEE Proceedings F (Radar and Signal Processing), 1992, **139**, (5), pp 343–350

[4] Stanković, L., Daković, M., Thayaparan, T., and Popović-Bugarin, V.: 'Micro-Doppler Removal in the Radar Imaging Analysis', IEEE Transactions on Aerospace and Electronic Systems, 2013, **49**, (2), pp 1234–1250

[5] Bai, X., Zhou, F., Xing, M., and Bao, Z.: 'High resolution ISAR imaging of targets with rotating parts', IEEE Transactions on Aerospace and Electronic Systems, 2011, **47**, (4), pp 2530–2543

[6] Totir, F., and Radoi, E.: 'Superresolution algorithms for spatial extended scattering centers', Digital Signal Processing, 2009, **19**, (5), pp 780–792

[7] Chen, V.C., Li, F., Ho, S.S., and Wechsler, H.: 'Micro-Doppler effect in radar: phenomenon, model, and simulation study', IEEE Transactions on Aerospace and Electronic Systems, 2006, **42**, (1), pp 2–21

[8] Sparr, T., Krane, B.: 'Micro-Doppler analysis of vibrating targets in SAR', IEE Proc. Radar Sonar Navig., 2003, **150**, (4), pp 277–283

[9] Martorella, M.: 'Novel approach for ISAR image cross-range scaling', IEEE Trans. Aerosp. Electron. Syst., 2008, **44**, (1), pp 281–294

[10] Stanković, L., Thayaparan, T., and Djurović, I.: 'Separation of target rigid body and micro-Doppler effects in ISAR imaging', IEEE Transactions on Aerospace and Electronic Systems, 2006, **41**, (4), pp 1496–1506

[11] Thayaparan, T., Abrol, S., Riseborough, E., Stanković, L., Lamothe, D., and Duff, G.: 'Analysis of radar micro-Doppler signatures from experimental helicopter and human data', IET Proceedings Radar Sonar and Navigation, 2007, **1**, (4), pp 288–299

[12] Thayaparan, T., Stanković, L., and Djurović, I.: 'Micro-Doppler Based Target Detection and Feature Extraction in Indoor and Outdoor Environments', Journal of the Franklin Institute, 2008, **345**, (6), pp 700–722

[13] Chen, V.C., Ling, H.: 'Time-frequency transforms for radar imaging and signal analysis' (Artech House, Boston, 2002)

[14] Wang, Y., Ling, H., and Chen, V.C.: 'ISAR motion compensation via adaptive joint time-frequency techniques', IEEE Transactions on Aerospace and Electronic Systems, 1998, **38**, (2), pp 670–677

[15] Djurović, I., Stanković, and L., Bohme, J.F.: 'Robust L-estimation based forms of signal transforms and time-frequency representations', IEEE Transactions on Signal Processing, 2003, **51**,(7), pp 1753–1761

[16] Stanković, L., Stanković, S., Orović, I., and Amin, M.: 'Robust Time-Frequency Analysis based on the L-estimation and Compressive Sensing', IEEE Signal Processing Letters, 2013, **20**, (5), pp 499–502

[17] Donoho, D.: 'Compressed sensing', IEEE Transactions on Information Theory, 2006, **52**, (4), pp 1289–1306

[18] Flandrin, P., Borgnat, P.: 'Time-Frequency Energy Distributions Meet Compressed Sensing', IEEE Transactions on Signal Processing, 2010, **58**, (6), pp 2974–2982.

[19] Stanković, L., Stanković, S., Orović, I., and Amin, M.: 'Compressive Sensing Based Separation of Non-Stationary and Stationary Signals Overlapping in Time-Frequency', IEEE Transactions on Signal Processing, 2013, **61**, (18), pp 4562–4572

[20] Stanković, L., Stanković, S., and Amin, M.: 'Missing Samples Analysis in Signals for Applications to L-Estimation and Compressive Sensing', Signal Processing, 2014, **94**, pp 401–408

[21] Stanković, L., Daković, M., and Thayaparan, T.: 'Time-Frequency Signal Analysis with Applications', (Artech House, Boston, 2013)

[22] Wang, Y., and Jiang, Y.C.: 'ISAR Imaging of Ship Target with Complex Motion Based on New Approach of Parameters Estimation for Polynomial Phase Signal', EURASIP Journal on Advances in Signal Processing, 2011, Article ID 425203

[23] Stanković, L.: 'A measure of some time-frequency distributions concentration', Signal Processing, 2001, **81**, (3), pp 621–631

[24] Sustik, M.A., Tropp, J.A., Dhillon, I.S., Heath, R.W.Jr.: 'On the existence of equiangular tight frames', Linear Algebra and its Applications, 2007, **426**, (2), pp 619–635

[25] Stanković, L., Stanković, S., Daković, M., and Orović, I.: 'Separation and Reconstruction of the Rigid Body and Micro-Doppler Signal in ISAR: Part II – Statistical Analysis', IET Radar, Sonar and Navigation, Special Issue: Micro Doppler

[26] Stanković, L.: 'On the ISAR Image Analysis and Recovery with Unavailable or Heavily Corrupted Data', IEEE Transactions on Aerospace and Electronic Systems, 2015, **51**, (3)